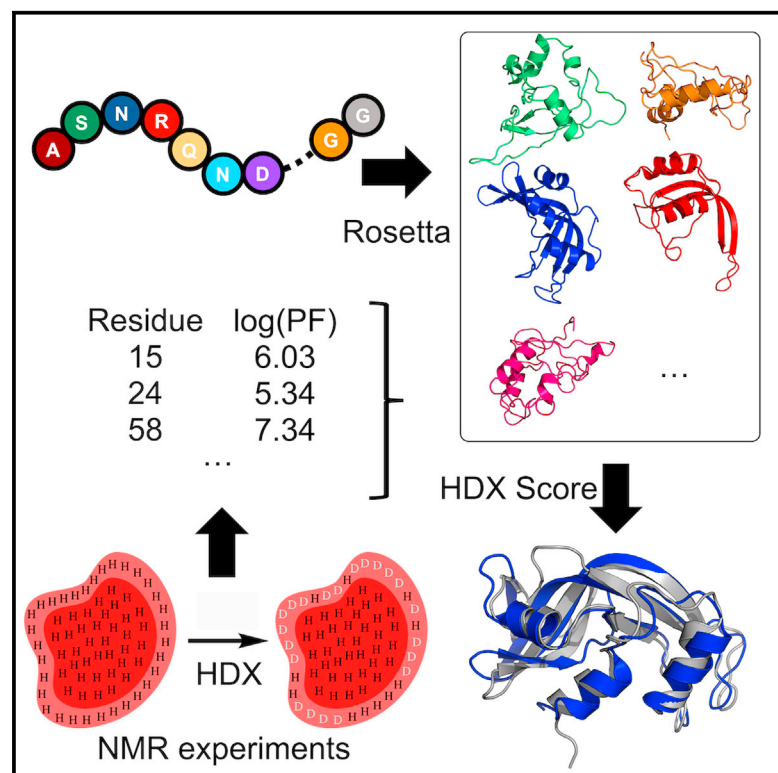


Structure

Protein structure prediction using residue-resolved protection factors from hydrogen-deuterium exchange NMR

Graphical abstract



Authors

Tung T. Nguyen, Daniel R. Marzolf,
Justin T. Seffernick, Sten Heinze,
Steffen Lindert

Correspondence

lindert.1@osu.edu

In brief

Nguyen et al. demonstrate structural correlations between protection factors, measured using HDX-NMR, and structural features of proteins, relating to solvent accessibility and flexibility. They then show that these correlations can be used to accurately predict structures using computational methods for 10 proteins.

Highlights

- Structural correlation between HDX-NMR PF and protein structure metrics
- Prediction of protein structure using HDX protection factors and Rosetta



Resource

Protein structure prediction using residue-resolved protection factors from hydrogen-deuterium exchange NMR

Tung T. Nguyen,² Daniel R. Marzolf,¹ Justin T. Seffernick,¹ Sten Heinze,¹ and Steffen Lindert^{1,3,*}¹Department of Chemistry and Biochemistry, Ohio State University, 2114 Newman & Wolfrom Laboratory, 100 W. 18th Avenue, Columbus, OH 43210, USA²Department of Chemistry and Biochemistry, Denison University, Granville, OH 43023, USA³Lead contact*Correspondence: lindert.1@osu.edu<https://doi.org/10.1016/j.str.2021.10.006>

SUMMARY

Hydrogen-deuterium exchange (HDX) measured by nuclear magnetic resonance (NMR) provides structural information for proteins relating to solvent accessibility and flexibility. While this structural information is beneficial, the data cannot be used exclusively to elucidate structures. However, the structural information provided by the HDX-NMR data can be supplemented by computational methods. In previous work, we developed an algorithm in Rosetta to predict structures using qualitative HDX-NMR data (categories of exchange rate). Here we expand on the effort, and utilize quantitative protection factors (PFs) from HDX-NMR for structure prediction. From observed correlations between PFs and solvent accessibility/flexibility measures, we present a scoring function to quantify the agreement with HDX data. Using a benchmark set of 10 proteins, an average improvement of 5.13 Å in root-mean-square deviation (RMSD) is observed for cases of inaccurate Rosetta predictions. Ultimately, seven out of 10 predictions are accurate without including HDX data, and nine out of 10 are accurate when using our PF-based HDX score.

INTRODUCTION

Protein function is encoded in the structure of the protein, allowing for understanding and manipulation of both mechanisms and function if the structure can be determined experimentally. However, experimental structure determination is challenging, particularly for more complex and disordered proteins, with some proteins eluding high-resolution structure determination due to their intrinsic properties. As a result, the gap between known protein sequences, which can be quickly determined, and known protein structures increases by the day. This gap is fueled by the difficulty of structural biology experiments, such as X-ray crystallography, cryogenic electron microscopy (cryo-EM), and ¹³C-, ¹⁵N-edited nuclear magnetic resonance (NMR) experiments, all of which have limitations associated with them (Ardenkjaer-Larsen et al., 2015; Lyumkis, 2019; Srivastava et al., 2018).

While tertiary structure has traditionally been determined using the aforementioned methodologies, in recent decades the advent of computational methods has led to potentially far higher-throughput structure prediction. With these predictions, however, come limitations such as increased probability of inaccurate *ab initio* structure predictions as protein size increases (Kim et al., 2009). The accuracy of computational methods can be significantly improved by the inclusion of experimental data (Seffernick and Lindert, 2020). Inclusion efforts began in the

1980s with NMR and X-ray crystallography, with more recent studies aiming toward including data from lower-resolution methods, such as electron paramagnetic resonance (EPR), mass spectrometry (MS), and cryo-EM (Alexander et al., 2008; Arahamian et al., 2018; Arahamian and Lindert, 2019; Biehn and Lindert, 2021; Bowers et al., 2000; DiMaio et al., 2015; Harvey et al., 2019; Lindert et al., 2012; Pilla et al., 2017; Roberts et al., 2017; Seffernick et al., 2019a; Srivastava et al., 2018; van Zundert et al., 2015). Ideally, these types of experimental data would be high-throughput and require a smaller sample size.

Biomolecular hydrogen-deuterium exchange (HDX) experiments, originating in the 1970s, have typically been used to map exchange rates onto atomic-resolution structures, elucidating dynamic properties using static models (Choe et al., 1998; Hooke et al., 1994; Palmer, 1997; Rosa and Richards, 1979). These studies have probed native-state dynamics on a diverse set of proteins, and have mapped protein folding pathways by performing the experiments as the molecule is (un)folding (Di Paolo et al., 2010; Rogov et al., 2004; Schulman et al., 1995). Determination of dynamic properties stem from a consensus that HDX rates are generally governed by exposure and flexibility of the amide protons, thus regions of faster exchange can be correlated to regions of higher flexibility and/or solvent exposure. Additionally, a wide variety of studies have



demonstrated the importance of accounting for dynamic properties by using sophisticated sampling methods (such as molecular dynamics simulations) to match structures to experimental data, as well as using these methods to better understand the factors influencing HDX (Best and Vendruscolo, 2006; Devaurs et al., 2017, 2018; Hilser and Freire, 1996; Makarov et al., 2020; Martens et al., 2019; McAllister and Konermann, 2015; Mohammadiarani et al., 2018; Petruk et al., 2013; Vendruscolo et al., 2003; Wan et al., 2020). Studies to simulate HDX data (Liu et al., 2012), reweigh model ensembles (Bradshaw et al., 2020; Craig et al., 2011; Wan et al., 2020), and evaluate protein-protein interactions (Borysik, 2017) require structural information and long, computationally expensive trajectories obtained from molecular dynamics simulations.

In absence of existing structural models, the data can also be used as restraints in computational protein structure prediction. Multiple studies have demonstrated that modeling based on agreement to HDX data measured from MS can be beneficial to enhance structural understanding of specific systems. For structure prediction of monomeric proteins from sequence, approaches using homology modeling along with HDX-MS data can be successful, even for systems that are difficult to crystallize (Ramsey et al., 2018; Zhang et al., 2014). Protein-protein docking has also been performed in combination with HDX-MS data, allowing for the prediction of complex structures in agreement with the data (Borysik, 2017; Roberts et al., 2017; Zhang et al., 2019).

In previous work, we have demonstrated that structural features relating to exposure and flexibility of amide protons are correlated to experimental HDX rates measured using NMR (Marzolf et al., 2021). Using a benchmark set of 38 proteins, a correlation between HDX rate and four calculated parameters related to exposure and flexibility was established. In brief, exposure was quantified using a calculated amide proton neighbor count (NC) and relative solvent-accessible surface area (RelSASA) (Arahamian et al., 2018). Flexibility was estimated using the order score (OS) (Kim et al., 2018; Seffernick et al., 2019b), a window-averaged residual Rosetta score, and hydrogen-bonding energies involving the amide proton. After developing a score term that evaluated agreement of the four parameters to experimental HDX rate categories in a large set of decoy structures, we were able to improve prediction accuracy, reducing root-mean-square deviation (RMSD) substantially. However, this scoring term used strength categories that corresponded to HDX rates rather than the quantitative exchange rates themselves, introducing a potential source of uncertainty.

In this report, we extend the methodologies from the previous work to directly employ quantitative HDX rates during the protein modeling using a benchmark set of 10 proteins. The quantitative rates, reported as protection factors (PFs), were used to predict parameters that related to exposure and flexibility. The predicted values were then compared with calculated values in models generated by Rosetta, with the difference in the values incorporated in a Rosetta scoring term. This method differs from our previous work (using quantitative PFs rather than categories of exchange) and other methods in the literature, which are generally used to match agreement for a single system (monomer or complex) using HDX-MS. In this report, we directly incorporated HDX rates measured from NMR experiments into a general

method, available in Rosetta, to predict monomer structure from sequence alone. Using this new scoring term, protein structure prediction accuracy increased, moving from 7 out of 10 to 9 out of 10 of the benchmark proteins predicting an accurate model (<5.5 Å RMSD to the native model) when the HDX data were included.

RESULTS AND DISCUSSION

Previous work showed HDX-NMR data provide useful information to structure prediction

Experimental data from HDX measured by NMR provide structural information on proteins. While this information alone cannot be used to fully elucidate the structures, it can be utilized as a supplement to computational prediction methods. Recently, we developed a method to use HDX-NMR data to predict tertiary structure from sequence using Rosetta *ab initio* structure prediction (Marzolf et al., 2021). In this previous work, the experimental data were categorized as strong, medium, or weak, corresponding to slow, medium, and fast exchange, respectively. The HDX score term was dependent on the following four residue-resolved metrics that were expected to influence the HDX rate: NC, RelSASA, hydrogen bond score (HB), and Rosetta OS, using ResidueDisorder (Kim et al., 2018; Seffernick et al., 2019b). In the previous study, structure prediction results improved when qualitative HDX data were included (Marzolf et al., 2021).

PFs provided more information for modeling and trends followed expected structural hypotheses

While results from previous work were promising and showed that a very small amount of experimental data can meaningfully improve prediction results, there was a potential to include more information from HDX-NMR experiments into structure prediction. In this study, rather than using qualitative data (where measured exchange rates were categorized into strong, medium, and weak), we used quantitative PFs measured from HDX-NMR experiments. PFs are defined as the ratio of the sequence-dependent intrinsic HDX rate constant to observed exchange rate constant. Residues (specifically backbone amide hydrogens) with higher PF (corresponding to lower relative exchange rate) are expected to be less flexible (i.e., participate strongly in hydrogen bonding) and/or have less exposure to the solvent. Similar to previous work, here we used HB and OS to quantify flexibility, and NC and RelSASA to quantify solvent exposure, but have done so using PFs.

Quantitative PFs were not as readily available as qualitative exchange rate categories for a large number of proteins. Our benchmark dataset contained 10 proteins (ranging from 76 to 223 residues; summarized in Table S1) for which experimental PFs were provided in the literature. For this dataset, we first sought to test our hypotheses (high exposure and high flexibility leading to increased exchange) by examining the correlations between the calculated residue-resolved parameters and PF. Figure 1 shows the NC, RelSASA, HB, and OS as a function of $\log(\text{PF})$ for residues in all 10 proteins (a total of 431 residues). The values of slopes and intercepts for each correlation are provided in Table S3. While the individual correlations did not appear to be exceptionally strong (R^2 of 0.12, 0.05, 0.05, and 0.04 respectively), the hypothesized trends were observed for

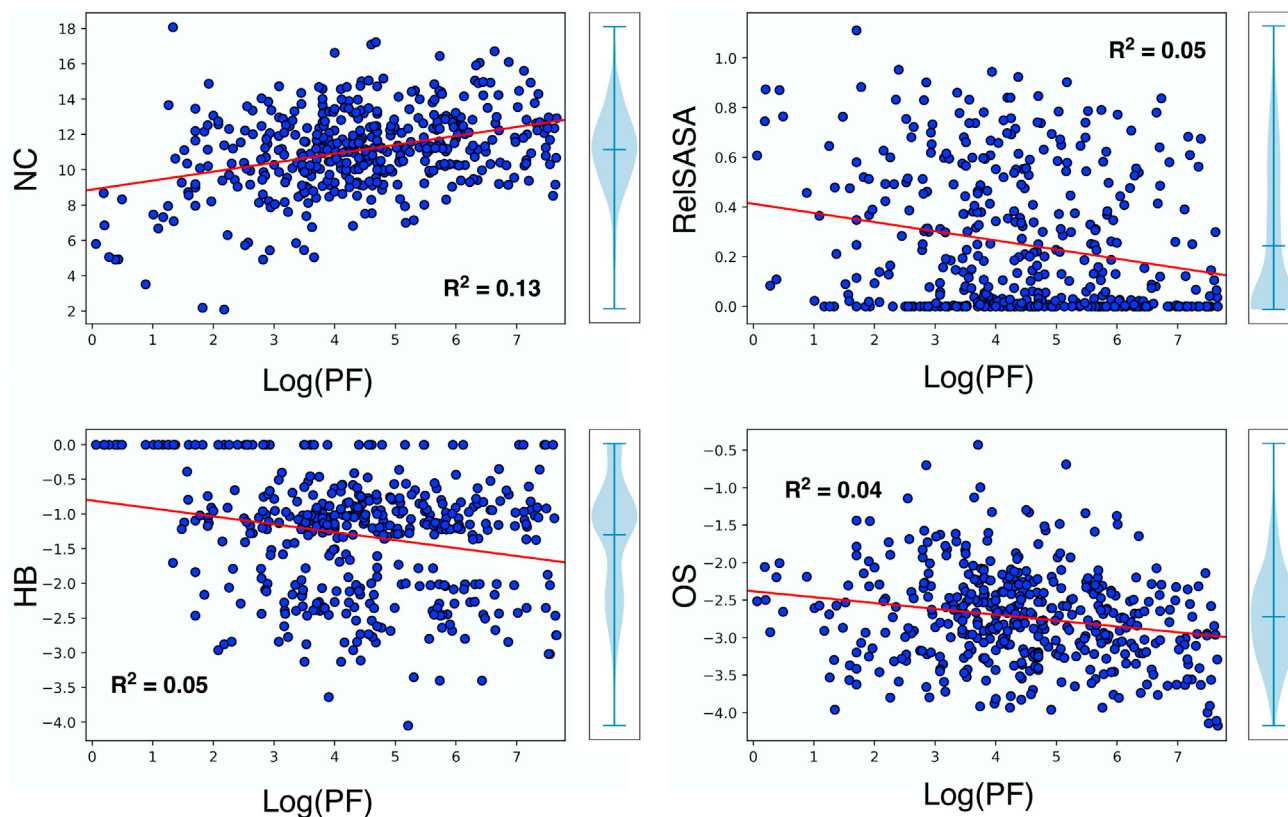


Figure 1. Experimental data correlations to structure

Correlations between the calculated structural parameters (NC, ReISASA, HB, and OS) with the log base 10 of HDX PF. Linear regression lines are shown in red along with the R^2 values. All trends matched structural hypotheses.

all four parameters. The relatively weak correlations were unsurprising because no individual parameter can be expected to govern exchange in a complex process such as HDX. Nonetheless, based on these native distributions, we developed a scoring function to be used to quantify the quality of a predicted protein structure based on its agreement with the NMR-HDX data.

Inclusion of HDX-NMR PF was beneficial for structure prediction

Rosetta *ab initio* structure prediction was used to predict structures from sequence for the majority of proteins in the dataset (8 out of 10). However, due to poor observed sampling, homology models were instead generated for 1SNO and 2ETL using RosettaCM. Regardless of method, 10,000 models were generated for each protein in the dataset and scored using the Rosetta REF2015 scoring function. For each protein, within the respective pool of models, structures with RMSD (with respect to the crystal structures) of less than 4 Å were sampled. The predicted structure without using HDX-NMR data was the lowest scoring model by Rosetta score. The accuracy of the predicted structures varied, with the RMSDs ranging from 0.67 Å to 14.75 Å, with 7 out of 10 less than 5.5 Å (see Figure 2).

To test the ability of HDX-NMR PFs to facilitate protein structure prediction, structures were also scored based on agreement with PF from HDX-NMR in addition to scoring with

Rosetta (HDX score). A detailed summary of the score is provided in the STAR Methods, but, in short, for each residue with a measured experimental PF, observed regression lines from Figure 1 (Table S3) were used to predict a value for all exposure and flexibility parameters respectively (NC, ReISASA, HB, and OS). Next, each predicted parameter was compared with the calculated parameter using the structure of the model. Based on the difference between observed and predicted parameters, each residue was scored in the range of -1 (good agreement, fully rewarded) and 0 (bad agreement, not rewarded). Using this function on all 100,000 generated models, $\sim 20\%$ of residues were fully rewarded (score of -1), $\sim 35\%$ were intermediately rewarded (score between -1 and 0), and $\sim 45\%$ of residues were not rewarded (score of 0). This distribution was similar to the distributions of the proteins individually, showing no strong bias for any one protein in the benchmark set. The HDX component of the scores for full protein structures was then derived by aggregating the agreement scores (referring to Equation 4) for each residue (with PF) and each parameter (NC, ReISASA, OS, and HB). While the scoring results using all four computational parameters are described in detail in the following paragraphs, we note that scoring with individual scoring terms was not as successful. This was not surprising, since single features were not expected to govern the complicated process of HDX. The scoring with individual terms was similar to or slightly worse than scoring with Rosetta only

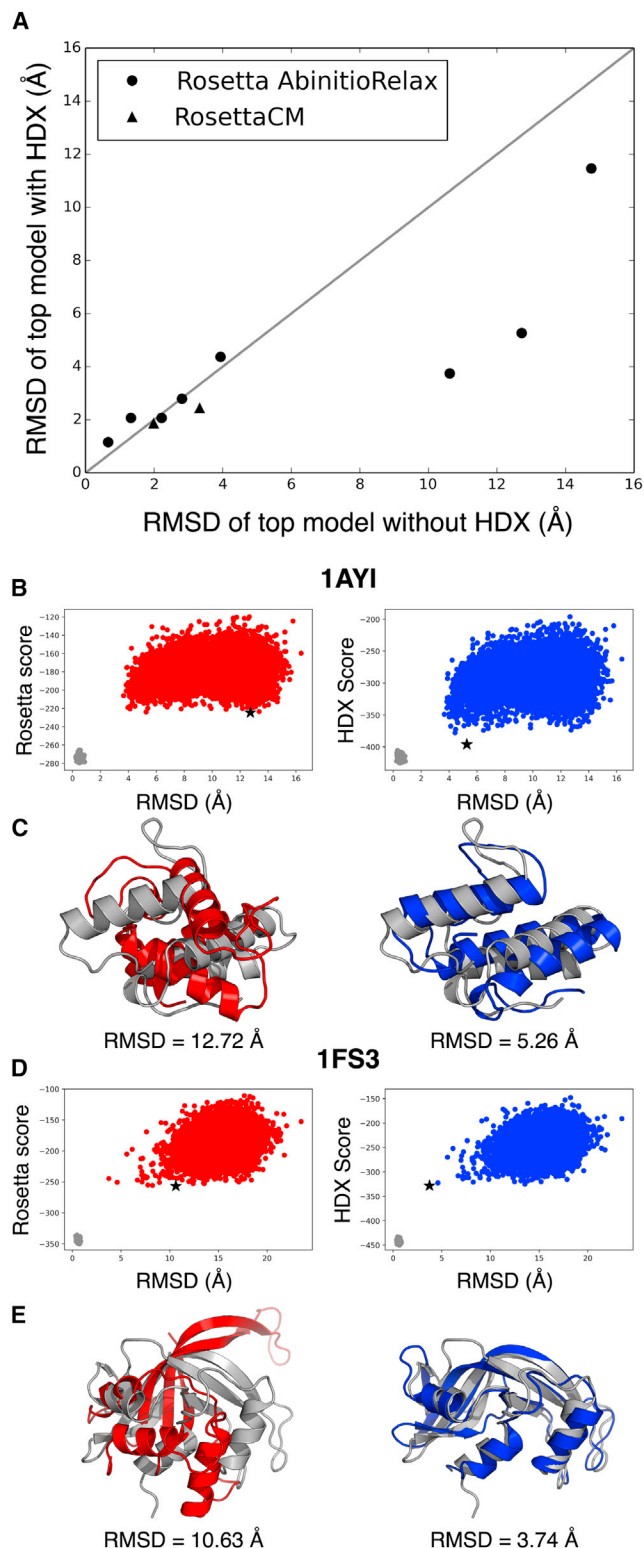


Figure 2. Comparison of prediction accuracy with and without HDX data

(A) RMSD of top scoring models with (y axis) and without (x axis) HDX data. Circles indicate structures predicted with *ab initio* and triangles indicate homology models.

(average RMSD of Rosetta only, 5.4 Å; average RMSD range using individual terms, 5.1–7.7 Å).

Ultimately, structures were scored using a combined score including both the Rosetta score and HDX component scores (based on agreement with HDX-NMR data) to get a consensus between the Rosetta energy function and experimental data (HDX score, referring to Equation 5). However, the HDX-dependent component of the HDX score performed remarkably well by itself as well (referring to the sum of HDX terms in Equation 5). For the majority of proteins in the dataset (7 out of 10), the top scoring model using only the HDX-dependent component of the HDX score was less than 5.5 Å, the same number as when scoring with Rosetta only (although a different set of seven). When using the HDX score, the RMSDs of all (10 out of 10) predicted structures were improved or were within 0.75 Å of the result obtained by scoring without experimental data. We also note that the results based on the relative weights between the four terms (NC, ReLSASA, OS, and HB) in Equation 5 were relatively stable with respect to small changes in weights. Figure 2A shows the RMSD of the predicted structures with and without including HDX data. Overall, the number of predicted structures with less than 5.5 Å RMSD improved to 9 out of 10 when HDX PFs were included (7 out of 10 without PF). The top scoring models were rewarded more by the individual HDX components of the score compared with the complete set of decoys: 27% fully rewarded, 40% intermediately rewarded, and 33% not rewarded.

Furthermore, two important features were observed: (1) for the seven proteins where Rosetta alone predicted an accurate structure (<5.5 Å RMSD), inclusion of HDX data did not significantly change prediction results (selected model RMSD changed by an average of 0.07 Å), and (2) for the three proteins where Rosetta alone predicted an inaccurate structure (1AY1, 1FS3, and 3BLG with RMSDs of 12.72 Å, 10.63 Å, and 14.75 Å, respectively), the inclusion of HDX data markedly improved the prediction results. The RMSD of the predicted model for each of these proteins improved by more than 3 Å with an average improvement of 5.13 Å when HDX data were included. This improvement compared favorably with our previous work (Marzolf et al., 2021), which used qualitative HDX-NMR data to predict structures (3.63 Å). We acknowledge that the dataset is too small (only three proteins met this criterion) to draw any universal conclusions. However, we hypothesize that more structural information is encoded in the quantitative HDX PF used in this work than the qualitative categories of exchange rates used in previous work. The additional information provided in the data may have contributed to the improved results. For two of these improved predictions (1AY1 and 1FS3), accurate structures were predicted when using HDX data; i.e., the RMSD of the final predicted structure was less than 5.5 Å. Figures 2B and 2D show the scores as a function of RMSD without (red) and with (blue) HDX data used for scoring 1AY1 and 1FS3, respectively. The predicted structures (i.e.,

(B and D) Score versus RMSD plots for 1AY1 and 1FS3 for Rosetta (red) and HDX score (blue). The predicted structure (lowest scoring model) is represented as a black star and 100 relaxed native structures are represented by gray circles.

(C and E) Predicted structures (Rosetta score, red; HDX score, blue) aligned to native (shown in gray).

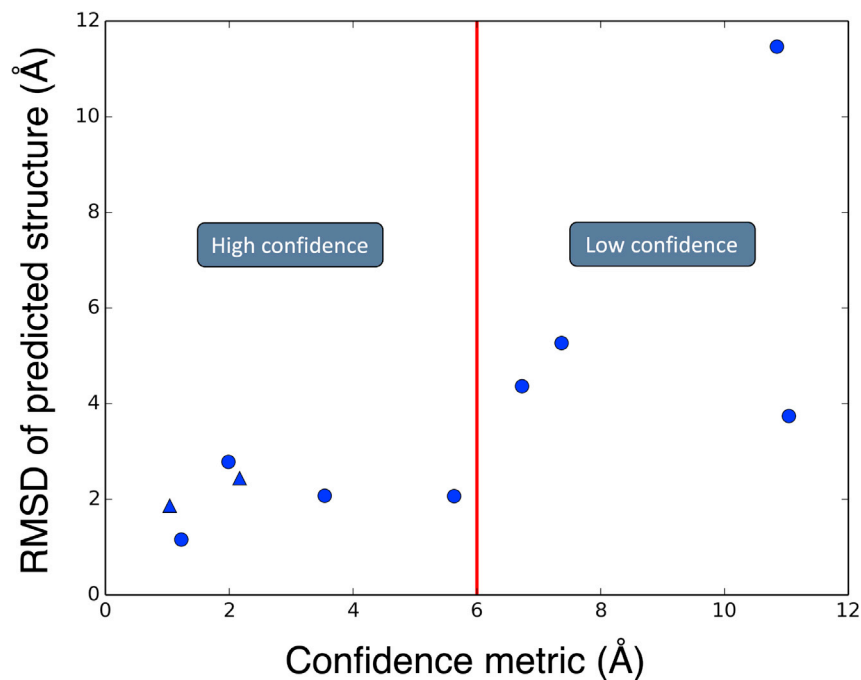


Figure 3. Confidence metric for analyzing prediction results

RMSD of predicted structure using HDX data for each protein shown along with the confidence metric (average RMSD of top 10 scoring models to top scoring model). Circles indicate structures predicted with *ab initio* and triangles indicate homology models. Vertical line shows separation between confidence regions: high confidence (less than 6 Å) and low confidence (greater than 6 Å). The confidence metric separated predictions well without knowledge of the native structure.

data for protein structure prediction. In this study, we extended this methodology to HDX-NMR data containing quantitative PFs. We demonstrated that these PFs correlated with structural features of proteins exhibiting the expected trends when modeled onto native crystal structures.

We then used these observed correlations of each parameter to develop a scoring function to quantify agreement between modeled structures and PF. When

models with the lowest score, corresponding to Figure 2A) are indicated with a star and those structures are shown aligned to the native crystal structures in Figures 2C and 2E. Similar score versus RMSD plots for the remaining eight proteins in the dataset are shown in Figure S1. From the *ab initio* sampling, the best RMSD structures were typically in the range of 2–5 Å (depending on the system). To demonstrate that the HDX score also ranked native-like structures well, we calculated the scores for 100 relaxed native structures (shown in the plots as gray circles). These data show that the HDX score did indeed identify these ~1-Å RMSD structures as native-like.

Confidence metric separated most native-like predictions from others

We sought to define a metric to assess the confidence of a prediction in the absence of a crystal structure. The confidence metric was defined as the average RMSD of the top 10 scoring models to the top scoring model. We hypothesized that this value would be lower when accurate predictions were made because a larger number of structures similar to the predicted structure would also score well. Using this metric, we were able to categorize our predictions as high confidence (<6 Å), or low confidence (>6 Å), as shown in Figure 3. This metric identified the top six predictions (all with RMSD less than 3 Å) as high confidence, while identifying the only prediction with RMSD >5.5 Å as low confidence. For high-confidence models, the average RMSD of the predicted structure was 2.06 Å, compared with 6.21 Å for low-confidence models.

Conclusion

HDX rates of backbone amide hydrogens measured by NMR provide structural information such as flexibility and solvent accessibility of backbone amide protons. In previous work, we developed a scoring function to utilize qualitative HDX-NMR

predicting tertiary structures of proteins using Rosetta, accurate structures (<5.5 Å RMSD of the predicted model) were predicted in 7 out of 10 cases. However, when quantitative PFs from HDX were included, 9 out of 10 of these benchmark cases were predicted accurately. For two cases, the RMSD of the predicted model improved by more than 6.5 Å when experimental data were included, and none of the accurate predictions were adversely affected by the HDX data (only changed by an average of 0.07 Å RMSD). Finally, we developed a confidence metric to identify the cases where our predicted structure was most likely to be native-like in the absence of knowledge of the crystal structure. This confidence metric correctly flagged the top six predictions as high confidence.

This work is an important extension of our previously developed HDX-NMR algorithm for protein structure prediction. These two algorithms now enable researchers to extract data from HDX-NMR as either qualitative categories or quantitative PFs to elucidate structures of proteins. Based on the relative ease of data collection for HDX-NMR, this computational method is beneficial. In this benchmark set, for all predictions where an inaccurate structure was predicted using Rosetta, the scoring based on HDX-NMR data improved the accuracy of the predicted structure. Based on our data, we speculate that the PFs from HDX-NMR provide information that can discriminate between correct and incorrect topology but do not contain enough information to refine near-atomic-resolution models. A tutorial on how to perform qualitative and quantitative HDX scoring with our algorithm in Rosetta has been included in the supplemental information (Method S1). In future work, we will extend our HDX methodology to study protein complexes. Additionally, we aim to utilize HDX data measured from MS (which has become more popular in recent years) and incorporate multiple types of experimental data to make more accurate predictions.

STAR★METHODS

Detailed methods are provided in the online version of this paper and include the following:

- KEY RESOURCES TABLE
- RESOURCE AVAILABILITY
 - Lead contact
 - Materials availability
 - Data and code availability
- EXPERIMENTAL MODEL AND SUBJECT DETAILS
- METHOD DETAILS
 - Benchmark dataset
 - Model generation
 - Calculations of HDX-dependent metrics
 - HDX agreement scores
 - Confidence metric
- QUANTIFICATION AND STATISTICAL ANALYSIS

SUPPLEMENTAL INFORMATION

Supplemental information can be found online at <https://doi.org/10.1016/j.str.2021.10.006>.

ACKNOWLEDGMENTS

We thank the members of the Lindert laboratory for many useful discussions. We would like to thank the Ohio Supercomputer Center for valuable computational resources (Ohio Supercomputer Center, 1987). Research reported in this publication, including the virtual summer Lindert laboratory internship by T.T.N., was supported by NSF (CHE 1750666).

AUTHOR CONTRIBUTIONS

T.T.N. collected data and analyzed results. D.M.H., J.T.S., and S.L. designed the project and assisted with data interpretation. S.H. and D.M.H. wrote and implemented Rosetta applications. All authors contributed to the manuscript preparation by way of writing (J.T.S., T.T.N., and D.M.H.), editing (J.T.S., T.T.N., D.M.H., S.H., and S.L.), and generating figures (J.T.S., T.T.N., and D.M.H.).

DECLARATION OF INTERESTS

The authors declare no competing interests.

Received: May 10, 2021

Revised: August 4, 2021

Accepted: October 15, 2021

Published: November 4, 2021

REFERENCES

- Alexander, N., Bortolus, M., Al-Mestarihi, A., McHaourab, H., and Meiler, J. (2008). De novo high-resolution protein structure determination from sparse spin-labeling EPR data. *Structure* *16*, 181–195. <https://doi.org/10.1016/j.str.2007.11.015>.
- Alford, R.F., Leaver-Fay, A., Jeliaskov, J.R., O'Meara, M.J., DiMaio, F.P., Park, H., Shapovalov, M.V., Renfrew, P.D., Mulligan, V.K., Kappel, K., et al. (2017). The Rosetta all-atom energy function for macromolecular modeling and design. *J. Chem. Theor. Comput.* *13*, 3031–3048. <https://doi.org/10.1021/acs.jctc.7b00125>.
- Aprahamian, M.L., and Lindert, S. (2019). Utility of covalent labeling mass spectrometry data in protein structure prediction with Rosetta. *J. Chem. Theor. Comput.* *15*, 3410–3424. <https://doi.org/10.1021/acs.jctc.9b00101>.
- Aprahamian, M.L., Chea, E.E., Jones, L.M., and Lindert, S. (2018). Rosetta protein structure prediction from hydroxyl radical protein footprinting mass spectrometry data. *Anal. Chem.* *90*, 7721–7729. <https://doi.org/10.1021/acs.analchem.8b01624>.
- Ardenkjaer-Larsen, J.H., Boebinger, G.S., Comment, A., Duckett, S., Edison, A.S., Engelke, F., Griesinger, C., Griffin, R.G., Hilty, C., Maeda, H., et al. (2015). Facing and overcoming sensitivity challenges in biomolecular NMR spectroscopy. *Angew. Chem. Int. Ed.* *54*, 9162–9185. <https://doi.org/10.1002/anie.201410653>.
- Bai, Y., Milne, J.S., Mayne, L., and Englander, S.W. (1993). Primary structure effects on peptide group hydrogen exchange. *Proteins* *17*, 75–86. <https://doi.org/10.1002/prot.340170110>.
- Best, R.B., and Vendruscolo, M. (2006). Structural interpretation of hydrogen exchange protection factors in proteins: characterization of the native state fluctuations of Cl2. *Structure* *14*, 97–106. <https://doi.org/10.1016/j.str.2005.09.012>.
- Bhuyan, A.K., and Udgaonkar, J.B. (1998). Two structural subdomains of barstar detected by rapid mixing NMR measurement of amide hydrogen exchange. *Proteins* *30*, 295–308.
- Biehn, S.E., and Lindert, S. (2021). Accurate protein structure prediction with hydroxyl radical protein footprinting data. *Nat. Commun.* *12*, 341. <https://doi.org/10.1038/s41467-020-20549-7>.
- Borysik, A.J. (2017). Simulated isotope exchange patterns enable protein structure determination. *Angew. Chem. Int. Ed.* *56*, 9396–9399. <https://doi.org/10.1002/anie.201704604>.
- Bowers, P.M., Strauss, C.E.M., and Baker, D. (2000). De novo protein structure determination using sparse NMR data. *J. Biomol. NMR* *18*, 311–318. <https://doi.org/10.1023/A:1026744431105>.
- Bradley, P., Misura, K.M., and Baker, D. (2005). Toward high-resolution de novo structure prediction for small proteins. *Science* *309*, 1868–1871. <https://doi.org/10.1126/science.1113801>.
- Bradshaw, R.T., Marinelli, F., Faraldo-Gómez, J.D., and Forrest, L.R. (2020). Interpretation of HDX data by maximum-entropy reweighting of simulated structural ensembles. *Biophys. J.* *118*, 1649–1664. <https://doi.org/10.1016/j.bpj.2020.02.005>.
- Chatani, E., Hayashi, R., Moriyama, H., and Ueki, T. (2002). Conformational strictness required for maximum activity and stability of bovine pancreatic ribonuclease A as revealed by crystallographic study of three Phe120 mutants at 1.4 Å resolution. *Protein Sci* *11*, 72–81. <https://doi.org/10.1110/ps.31102>.
- Choe, S.E., Matsudaira, P.T., Osterhout, J., Wagner, G., and Shakhnovich, E.I. (1998). Folding kinetics of villin 14T, a protein domain with a central beta-sheet and two hydrophobic cores. *Biochemistry* *37*, 14508–14518. <https://doi.org/10.1021/bi980889k>.
- Craig, P.O., Lätzer, J., Weinkam, P., Hoffman, R.M., Ferreira, D.U., Komives, E.A., and Wolynes, P.G. (2011). Prediction of native-state hydrogen exchange from perfectly funneled energy landscapes. *J. Am. Chem. Soc.* *133*, 17463–17472. <https://doi.org/10.1021/ja207506z>.
- Das, C., Hoang, Q.Q., Kreinbring, C.A., Luchansky, S.J., Meray, R.K., Ray, S.S., Lansbury, P.T., Ringe, D., and Petsko, G.A. (2006). Structural basis for conformational plasticity of the Parkinson's disease-associated ubiquitin hydrolase UCH-L1. *Proc Natl Acad Sci U S A* *103*, 4675–4680. <https://doi.org/10.1073/pnas.0510403103>.
- Dennis, C.A., Videler, H., Pauptit, R.A., Wallis, R., James, R., Moore, G.R., and Kleanthous, C. (1998). A structural comparison of the colicin immunity proteins Im7 and Im9 gives new insights into the molecular determinants of immunity-protein specificity. *Biochem J* *333* (Pt 1), 183–191. <https://doi.org/10.1042/bj3330183>.
- Devaurs, D., Antunes, D.A., Papanastasiou, M., Moll, M., Ricklin, D., Lambris, J.D., and Kavraki, L.E. (2017). Coarse-grained conformational sampling of protein structure improves the fit to experimental hydrogen-exchange data. *Front. Mol. Biosci.* *4*, 13. <https://doi.org/10.3389/fmolb.2017.00013>.
- Devaurs, D., Papanastasiou, M., Antunes, D.A., Abella, J.R., Moll, M., Ricklin, D., Lambris, J.D., and Kavraki, L.E. (2018). Native state of complement protein C3d analysed via hydrogen exchange and conformational sampling. *Int. J.*

- Comput. Biol. Drug Des. 11, 90–113. <https://doi.org/10.1504/jcbdd.2018.090834>.
- Di Paolo, A., Balbeur, D., De Pauw, E., Redfield, C., and Matagne, A. (2010). Rapid collapse into a molten globule is followed by simple two-state kinetics in the folding of lysozyme from bacteriophage λ . *Biochemistry* 49, 8646–8657. <https://doi.org/10.1021/bi101126f>.
- DiMaio, F., Song, Y., Li, X., Brunner, M.J., Xu, C., Conticello, V., Egelman, E., Marlovits, T., Cheng, Y., and Baker, D. (2015). Atomic-accuracy models from 4.5-Å cryo-electron microscopy data with density-guided iterative local refinement. *Nat. Methods* 12, 361–365. <https://doi.org/10.1038/nmeth.3286>.
- Forge, V., Hoshino, M., Kuwata, K., Arai, M., Kuwajima, K., Batt, C.A., and Goto, Y. (2000). Is folding of beta-lactoglobulin non-hierarchical? Intermediate with native-like beta-sheet and non-native alpha-helix. *J. Mol. Biol.* 296, 1039–1051. <https://doi.org/10.1006/jmbi.1999.3515>.
- Harvey, S.R., Seffernick, J.T., Quintyn, R.S., Song, Y., Ju, Y., Yan, J., Sahasrabudhe, A.N., Norris, A., Zhou, M., Behrman, E.J., et al. (2019). Relative interfacial cleavage energetics of protein complexes revealed by surface collisions. *Proc. Natl. Acad. Sci. U S A* 116, 8143–8148. <https://doi.org/10.1073/pnas.1817632116>.
- Hilser, V.J., and Freire, E. (1996). Structure-based calculation of the equilibrium folding pathway of proteins. Correlation with hydrogen exchange protection factors. *J. Mol. Biol.* 262, 756–772. <https://doi.org/10.1006/jmbi.1996.0550>.
- Hooke, S.D., Radford, S.E., and Dobson, C.M. (1994). The refolding of human lysozyme: a comparison with the structurally homologous hen lysozyme. *Biochemistry* 33, 5867–5876. <https://doi.org/10.1021/bi00185a026>.
- Johnson, M., Zaretskaya, I., Raytselis, Y., Merezukh, Y., McGinnis, S., and Madden, T.L. (2008). NCBI BLAST: a better web interface. *Nucleic Acids Res.* 36, W5–W9. <https://doi.org/10.1093/nar/gkn201>.
- Kim, D.E., Chivian, D., and Baker, D. (2004). Protein structure prediction and analysis using the Robetta server. *Nucleic Acids Res.* 32, W526–W531. <https://doi.org/10.1093/nar/gkh468>.
- Kim, D.E., Blum, B., Bradley, P., and Baker, D. (2009). Sampling bottlenecks in de novo protein structure prediction. *J. Mol. Biol.* 393, 249–260. <https://doi.org/10.1016/j.jmb.2009.07.063>.
- Kim, S.S., Seffernick, J.T., and Lindert, S. (2018). Accurately predicting disordered regions of proteins using Rosetta ResidueDisorder application. *J. Phys. Chem. B* 122, 3920–3930. <https://doi.org/10.1021/acs.jpcc.8b01763>.
- Lacroix, E., Bruix, M., López-Hernández, E., Serrano, L., and Rico, M. (1997). Amide hydrogen exchange and internal dynamics in the chemotactic protein CheY from *Escherichia coli*. *J. Mol. Biol.* 271, 472–487. <https://doi.org/10.1006/jmbi.1997.1178>.
- Leaver-Fay, A., Tyka, M., Lewis, S.M., Lange, O.F., Thompson, J., Jacak, R., Kaufman, K., Renfrew, P.D., Smith, C.A., Sheffler, W., et al. (2011). ROSETTA3: an object-oriented software suite for the simulation and design of macromolecules. *Methods Enzymol.* 487, 545–574. <https://doi.org/10.1016/b978-0-12-381270-4.00019-6>.
- Leman, J.K., Weitzner, B.D., Lewis, S.M., Adolf-Bryfogle, J., Alam, N., Alford, R.F., Aprahamian, M., Baker, D., Barlow, K.A., Barth, P., et al. (2020). Macromolecular modeling and design in Rosetta: recent methods and frameworks. *Nat. Methods* 17, 665–680. <https://doi.org/10.1038/s41592-020-0848-2>.
- Lindert, S., Hofmann, T., Wötzel, N., Karakaş, M., Stewart, P.L., and Meiler, J. (2012). Ab initio protein modeling into CryoEM density maps using EM-Fold. *Biopolymers* 97, 669–677. <https://doi.org/10.1002/bip.22027>.
- Liu, T., Pantazatos, D., Li, S., Hamuro, Y., Hilser, V.J., and Woods, V.L., Jr. (2012). Quantitative assessment of protein structural models by comparison of H/D exchange MS data with exchange behavior accurately predicted by DXCOREX. *J. Am. Soc. Mass Spectrom.* 23, 43–56. <https://doi.org/10.1007/s13361-011-0267-9>.
- Lou, S.C., Wetzel, S., Zhang, H., Crone, E.W., Lee, Y.T., Jackson, S.E., and Hsu, S.D. (2016). The knotted protein UCH-L1 exhibits partially unfolded forms under native conditions that share common structural features with its kinetic folding intermediates. *J. Mol. Biol.* 428, 2507–2520. <https://doi.org/10.1016/j.jmb.2016.04.002>.
- Lubienski, M.J., Bycroft, M., Freund, S.M., and Fersht, A.R. (1994). Three-dimensional solution structure and ¹³C assignments of barstar using nuclear magnetic resonance spectroscopy. *Biochemistry* 33, 8866–8877.
- Lyumkis, D. (2019). Challenges and opportunities in cryo-EM single-particle analysis. *J. Biol. Chem.* 294, 5181–5197. <https://doi.org/10.1074/jbc.REV118.005602>.
- Makarov, A.A., Iacob, R.E., Pirrone, G.F., Rodriguez-Granillo, A., Joyce, L., Mangion, I., Moore, J.C., Sherer, E.C., and Engen, J.R. (2020). Combination of HDX-MS and in silico modeling to study enzymatic reactivity and stereoselectivity at different solvent conditions. *J. Pharm. Biomed. Anal.* 182, 113141. <https://doi.org/10.1016/j.jpba.2020.113141>.
- Martens, C., Shekhar, M., Lau, A.M., Tajkhorshid, E., and Politis, A. (2019). Integrating hydrogen-deuterium exchange mass spectrometry with molecular dynamics simulations to probe lipid-modulated conformational changes in membrane proteins. *Nat. Protoc.* 14, 3183–3204. <https://doi.org/10.1038/s41596-019-0219-6>.
- Martin, C., Richard, V., Salem, M., Hartley, R., and Mauguen, Y. (1999). Refinement and structural analysis of barnase at 1.5 Å resolution. *Acta Crystallogr D Biol Crystallogr* 55, 386–398. <https://doi.org/10.1107/S0907444998010865>.
- Marzolf, D.R., Seffernick, J.T., and Lindert, S. (2021). Protein structure prediction from NMR hydrogen-deuterium exchange data. *J. Chem. Theor. Comput.* 17, 2619–2629. <https://doi.org/10.1021/acs.jctc.1c00077>.
- McAllister, R.G., and Konermann, L. (2015). Challenges in the interpretation of protein h/d exchange data: a molecular dynamics simulation perspective. *Biochemistry* 54, 2683–2692. <https://doi.org/10.1021/acs.biochem.5b00215>.
- Mohammadiarani, H., Shaw, V.S., Neubig, R.R., and Vashisth, H. (2018). Interpreting hydrogen-deuterium exchange events in proteins using atomistic simulations: case studies on regulators of G-protein signaling proteins. *J. Phys. Chem. B* 122, 9314–9323. <https://doi.org/10.1021/acs.jpcc.8b07494>.
- Ohio Supercomputer Center (1987). Ohio Supercomputer Center.
- Palmer, A.G., 3rd (1997). Probing molecular motion by NMR. *Curr. Opin. Struct. Biol.* 7, 732–737. [https://doi.org/10.1016/s0959-440x\(97\)80085-1](https://doi.org/10.1016/s0959-440x(97)80085-1).
- Pan, Y., and Briggs, M.S. (1992). Hydrogen exchange in native and alcohol forms of ubiquitin. *Biochemistry* 31, 11405–11412. <https://doi.org/10.1021/bi00161a019>.
- Perrett, S., Clarke, J., Hounslow, A.M., and Fersht, A.R. (1995). Relationship between equilibrium amide proton exchange behavior and the folding pathway of barnase. *Biochemistry* 34, 9288–9298. <https://doi.org/10.1021/bi00029a003>.
- Petruk, A.A., Defelipe, L.A., Rodríguez Limardo, R.G., Bucci, H., Marti, M.A., and Turjanski, A.G. (2013). Molecular dynamics simulations provide atomistic insight into hydrogen exchange mass spectrometry experiments. *J. Chem. Theor. Comput.* 9, 658–669. <https://doi.org/10.1021/ct300519v>.
- Pilla, K.B., Gaalswyk, K., and MacCallum, J.L. (2017). Molecular modeling of biomolecules by paramagnetic NMR and computational hybrid methods. *Biochim. Biophys. Acta Protein Proteomics* 1865, 1654–1663. <https://doi.org/10.1016/j.bbapap.2017.06.016>.
- Qin, B.Y., Bewley, M.C., Creamer, L.K., Baker, H.M., Baker, E.N., and Jameson, G.B. (1998). Structural basis of the Tanford transition of bovine beta-lactoglobulin. *Biochemistry* 37, 14014–14023. <https://doi.org/10.1021/bi981016t>.
- Radisky, E.S., Kwan, G., Karen Lu, C.J., and Koshland, D.E., Jr. (2004). Binding, proteolytic, and crystallographic analyses of mutations at the protease-inhibitor interface of the subtilisin BPN'/chymotrypsin inhibitor 2 complex. *Biochemistry* 43, 13648–13656. <https://doi.org/10.1021/bi048797k>.
- Ramsey, K.M., Narang, D., and Komives, E.A. (2018). Prediction of the presence of a seventh ankyrin repeat in IκBε from homology modeling combined with hydrogen-deuterium exchange mass spectrometry (HDX-MS). *Protein Sci.* 27, 1624–1635. <https://doi.org/10.1002/pro.3459>.
- Roberts, V.A., Pique, M.E., Hsu, S., and Li, S. (2017). Combining H/D exchange mass spectrometry and computational docking to derive the structure of

- protein-protein complexes. *Biochemistry* 56, 6329–6342. <https://doi.org/10.1021/acs.biochem.7b00643>.
- Rogov, V.V., Bernhard, F., Löhr, F., and Dötsch, V. (2004). Solution structure of the *Escherichia coli* YojN histidine-phosphotransferase domain and its interaction with cognate phosphoryl receiver domains. *J. Mol. Biol.* 343, 1035–1048. <https://doi.org/10.1016/j.jmb.2004.08.096>.
- Rosa, J.J., and Richards, F.M. (1979). An experimental procedure for increasing the structural resolution of chemical hydrogen-exchange measurements on proteins: application to ribonuclease S peptide. *J. Mol. Biol.* 133, 399–416. [https://doi.org/10.1016/0022-2836\(79\)90400-5](https://doi.org/10.1016/0022-2836(79)90400-5).
- Santoro, J., Bruix, M., Pascual, J., López, E., Serrano, L., and Rico, M. (1995). Three-dimensional structure of chemotactic Che Y protein in aqueous solution by nuclear magnetic resonance methods. *J. Mol. Biol.* 247, 717–725. <https://doi.org/10.1006/jmbi.1995.0175>.
- Schulman, B.A., Redfield, C., Peng, Z.Y., Dobson, C.M., and Kim, P.S. (1995). Different subdomains are most protected from hydrogen exchange in the molten globule and native states of human alpha-lactalbumin. *J. Mol. Biol.* 253, 651–657. <https://doi.org/10.1006/jmbi.1995.0579>.
- Seffernick, J.T., and Lindert, S. (2020). Hybrid methods for combined experimental and computational determination of protein structure. *J. Chem. Phys.* 153, 240901. <https://doi.org/10.1063/5.0026025>.
- Seffernick, J.T., Harvey, S.R., Wysocki, V.H., and Lindert, S. (2019a). Predicting protein complex structure from surface-induced dissociation mass spectrometry data. *ACS Cent. Sci.* 5, 1330–1341. <https://doi.org/10.1021/acscentsci.8b00912>.
- Seffernick, J.T., Ren, H., Kim, S.S., and Lindert, S. (2019b). Measuring intrinsic disorder and tracking conformational transitions using Rosetta ResidueDisorder. *J. Phys. Chem. B* 123, 7103–7112. <https://doi.org/10.1021/acs.jpcc.9b04333>.
- Sievers, F., and Higgins, D.G. (2018). Clustal Omega for making accurate alignments of many protein sequences. *Protein Sci.* 27, 135–145. <https://doi.org/10.1002/pro.3290>.
- Simons, K.T., Kooperberg, C., Huang, E., and Baker, D. (1997). Assembly of protein tertiary structures from fragments with similar local sequences using simulated annealing and Bayesian scoring functions. *J. Mol. Biol.* 268, 209–225. <https://doi.org/10.1006/jmbi.1997.0959>.
- Skinner, J.J., Lim, W.K., Bédard, S., Black, B.E., and Englander, S.W. (2012). Protein hydrogen exchange: testing current models. *Protein Sci.* 21, 987–995. <https://doi.org/10.1002/pro.2082>.
- Song, Y., DiMaio, F., Wang, R.Y., Kim, D., Miles, C., Brunette, T., Thompson, J., and Baker, D. (2013). High-resolution comparative modeling with RosettaCM. *Structure* 21, 1735–1742. <https://doi.org/10.1016/j.str.2013.08.005>.
- Srivastava, A., Nagai, T., Miyashita, O., and Tama, F. (2018). Role of computational methods in going beyond X-ray crystallography to explore protein structure and dynamics. *Int. J. Mol. Sci.* 19. <https://doi.org/10.3390/ijms19113401>.
- Truckses, D.M., Somoza, J.R., Prehoda, K.E., Miller, S.C., and Markley, J.L. (1996). Coupling between trans/cis proline isomerization and protein stability in staphylococcal nuclease. *Protein Sci* 5, 1907–1916. <https://doi.org/10.1002/pro.5560050917>.
- Vadas, O., and Burke, J.E. (2015). Probing the dynamic regulation of peripheral membrane proteins using hydrogen deuterium exchange-MS (HDX-MS). *Biochem. Soc. Trans.* 43, 773–786. <https://doi.org/10.1042/bst20150065>.
- van Zundert, G.C.P., Melquiond, A.S.J., and Bonvin, A. (2015). Integrative modeling of biomolecular complexes: HADDOCKing with cryo-electron microscopy data. *Structure* 23, 949–960. <https://doi.org/10.1016/j.str.2015.03.014>.
- Vendruscolo, M., Paci, E., Dobson, C.M., and Karplus, M. (2003). Rare fluctuations of native proteins sampled by equilibrium hydrogen exchange. *J. Am. Chem. Soc.* 125, 15686–15687. <https://doi.org/10.1021/ja036523z>.
- Vijay-Kumar, S., Bugg, C.E., and Cook, W.J. (1987). Structure of ubiquitin refined at 1.8 Å resolution. *J. Mol. Biol.* 194, 531–544. [https://doi.org/10.1016/0022-2836\(87\)90679-6](https://doi.org/10.1016/0022-2836(87)90679-6).
- Wan, H., Ge, Y., Razavi, A., and Voelz, V.A. (2020). Reconciling simulated ensembles of apomyoglobin with experimental hydrogen/deuterium exchange data using bayesian inference and multiensemble Markov state models. *J. Chem. Theor. Comput.* 16, 1333–1348. <https://doi.org/10.1021/acs.jctc.9b01240>.
- Wang, A., Robertson, A.D., and Bolen, D.W. (1995). Effects of a naturally occurring compatible osmolyte on the internal dynamics of ribonuclease A. *Biochemistry* 34, 15096–15104. <https://doi.org/10.1021/bi00046a016>.
- Zhang, Y., Majumder, E.L., Yue, H., Blankenship, R.E., and Gross, M.L. (2014). Structural analysis of diheme cytochrome c by hydrogen-deuterium exchange mass spectrometry and homology modeling. *Biochemistry* 53, 5619–5630. <https://doi.org/10.1021/bi500420y>.
- Zhang, M.M., Beno, B.R., Huang, R.Y., Adhikari, J., Deyanova, E.G., Li, J., Chen, G., and Gross, M.L. (2019). An integrated approach for determining a protein-protein binding interface in solution and an evaluation of hydrogen-deuterium exchange kinetics for adjudicating candidate docking models. *Anal. Chem.* 91, 15709–15717. <https://doi.org/10.1021/acs.analchem.9b03879>.

STAR★METHODS

KEY RESOURCES TABLE

REAGENT or RESOURCE	SOURCE	IDENTIFIER
Deposited data		
Structure of barnase	(Martin et al., 1999)	PDB: 1A2P
Structure of colicin E immunity protein 7	(Dennis et al., 1998)	PDB: 1AYI
Structure of barstar	(Lubienski et al., 1994)	PDB: 1BTA
Structure of che Y	(Santoro et al., 1995)	PDB: 1CYE
Structure of bovine pancreatic ribonuclease A	(Chatani et al., 2002)	PDB: 1FS3
Structure of staphylococcal nuclease	(Truckses et al., 1996)	PDB: 1SNO
Structure of chymotrypsin inhibitor 2	(Radisky et al., 2004)	PDB: 1TM1
Structure of ubiquitin	(Vijay-Kumar et al., 1987)	PDB: 1UBQ
Structure of ubiquitin carboxyl-terminal hydrolase isozyme L1	(Das et al., 2006)	PDB: 2ETL
Structure of beta-lactoglobulin	(Qin et al., 1998)	PDB: 3BLG
Software and algorithms		
Rosetta	(Leman et al., 2020)	https://www.rosettacommons.org/software/academic
Rosetta AbinitioRelax	(Bradley et al., 2005)	https://www.rosettacommons.org/docs/latest/application_documentation/structure_prediction/abinitio-relax
RosettaCM	(Song et al., 2013)	https://www.rosettacommons.org/docs/latest/application_documentation/structure_prediction/RosettaCM
Robetta web server	(Kim et al., 2004)	http://old.robetta.org/
Standard Protein BLAST	(Johnson et al., 2008)	https://blast.ncbi.nlm.nih.gov/Blast.cgi
Clustal Omega	(Sievers and Higgins, 2018)	https://www.ebi.ac.uk/Tools/msa/clustalo/

RESOURCE AVAILABILITY

Lead contact

Further information and requests for resources should be directed to and will be fulfilled by the lead contact, Steffen Lindert (lindert.1@osu.edu).

Materials availability

This study did not generate new unique reagents.

Data and code availability

The HDXEnergy application has been contributed to Rosetta software, and a tutorial for running the application is available in the [supplemental information \(Method S1\)](#). All model generation and residual property calculations were performed within the Rosetta software framework, available free for educational purposes at <https://www.rosettacommons.org/software>. All protein structure and sequence files are available in the Protein Data Bank (PDB) at <https://www.rcsb.org/>. Residual protection factors can be found in the Excel file provided in the [supplemental information \(Data S1\)](#). All software and algorithms used in this paper are available and listed in the [key resources table](#). Any additional information required to reanalyze the data reported in this paper is available from the lead contact upon request.

EXPERIMENTAL MODEL AND SUBJECT DETAILS

All data were generated from the datasets provided in the KRT.

METHOD DETAILS

Benchmark dataset

In this work, we used HDX-NMR protection factors (PFs), which are dependent on solvent accessibility and structural flexibility of specific residues (Bai et al., 1993). For a residue, protection factor is defined as a ratio between the intrinsic HDX rate constant (k_{int}) and the observed HDX rate constant (k_{ex}) as shown in Equation 1 (Bai et al., 1993; Perrett et al., 1995):

$$PF = \frac{k_{int}}{k_{ex}} \quad (\text{Equation 1})$$

The benchmark dataset for this study contained ten proteins with reported residue-resolved HDX-NMR protection factors which were all consistent with the definition in Equation 1. While a detailed summary of the benchmark set is shown in Table S1, in short, the proteins used in this study were barnase (PDB: 1A2P), colicin E immunity protein 7 (PDB: 1AYI), barstar (PDB: 1BTA), che Y (PDB: 1CYE), bovine pancreatic ribonuclease A (PDB: 1FS3), staphylococcal nuclease (PDB: 1SNO), chymotrypsin inhibitor 2 (PDB: 1TM1), ubiquitin (PDB: 1UBQ), ubiquitin carboxyl-terminal hydrolase isozyme L1 (PDB: 2ETL), and beta-lactoglobulin (PDB: 3BLG). All ten proteins were monomers and experimentally determined structures were available in the Protein Data Bank (PDB). The total number of residues of these proteins ranged from 64 to 223 (Table S1). For 1A2P, 1FS3, and 2ETL, the HDX experiments were conducted at various pHs. The protection factors for the most acidic pH were selected for each protein [pH = 6.5 for 1A2P (Perrett et al., 1995), pH = 6.5 for 1FS3 (Wang et al., 1995), and pH = 7.6 for 2ETL (Lou et al., 2016)]. In our benchmark dataset, five proteins were reported with the raw protection factors [1A2P (Perrett et al., 1995), 1BTA (Bhuyan and Udgaonkar, 1998), 1FS3 (Wang et al., 1995), 1UBQ (Pan and Briggs, 1992), and 3BLG (Forge et al., 2000)], three proteins were reported with the logarithmic base 10 of protection factors [1CYE (Lacroix et al., 1997), 1SNO (Devaurs et al., 2017; Skinner et al., 2012), and 2ETL (Lou et al., 2016)], and two proteins were reported with the natural logarithm of protection factors [1AYI (Devaurs et al., 2017) and 1TM1 (Devaurs et al., 2017)]. Thus, to standardize protection factors and calculations, all the values were converted into logarithm with base 10 of raw protection factors ($\log[PF]$).

Model generation

To assess the competence of the developed HDX scoring function to distinguishing near-native models from other decoy models, the decoy set must have a wide distribution of RMSDs (root-mean square deviation to crystal structures), ranging from near-native models (<4 Å RMSD) to models with incorrect topology (>8 Å RMSD). For the majority of proteins in the benchmark dataset, to achieve this purpose, we generated 10,000 decoy models using the standard Rosetta AbinitioRelax protocol (Leaver-Fay et al., 2011; Simons et al., 1997). The Robetta Web server was used to generate the 3-mer and 9-mer fragment files (Kim et al., 2004). The REF2015 scoring function (Alford et al., 2017) was used to score each model for its conformational stability, and the RMSD to the relaxed native structure was calculated for each of the generated models. For 1BTA, 1CYE, 1TM1, 1UBQ, and 3BLG, we used the fragment files generated by excluding homologs. However, for 1A2P, 1AYI, and 1FS3, due to poor model sampling, (none of the models generated were considered near-native) fragment files were generated by including homologs.

Likewise, because of poor observed sampling of the Rosetta AbinitioRelax protocol (both with and without homologous fragments), for 1SNO and 2ETL, the RosettaCM protocol was applied to generate 10,000 decoy homology models of the target proteins (Song et al., 2013). The Standard Protein BLAST server (using the Position-Specific Iterated BLAST) was used to search for different protein sequences with various query coverage and percent identity to the target protein (Johnson et al., 2008). For 1SNO, 3SK6 and 2W8U were selected as templates, while for 2ETL, the templates were 1UCH and 3IHR. Percent identity, coverage, and similarity for each template are shown in Table S2. The templates were aligned with the targets (1SNO and 2ETL) using the Clustal Omega server (Sievers and Higgins, 2018). From the alignment, the sequence of the target was threaded onto each template. Finally, 10,000 decoy models were generated by hybridizing the threaded target sequence on templates with different weights (Table S2).

Calculations of HDX-dependent metrics

The HDX rate for each residue was expected to correlate with flexibility and solvent exposure (Vadas and Burke, 2015). Neighbor count (NC) and relative solvent accessible surface area (RelSASA) were used to quantify solvent accessibility, and order score (OS) and hydrogen bond energy (HB) were used to quantify flexibility. Calculations of each of these four metrics were thoroughly described in our previous work (Marzolf et al., 2021). In short, NC was based on the number of oxygen atoms in the proximity of the amide protons (based on distance and angular cutoffs). RelSASA quantified the solvent accessibility of the side-chain atoms by calculating the ratio between the measured SASA and the theoretical maximum SASA. OS was a window averaged Rosetta residue score, representing the disorder of a residue (Kim et al., 2018; Seffernick et al., 2019b). Finally, HB was the hydrogen bonding energy of interactions between the amide proton and other residues. All four metrics were calculated using Rosetta applications.

HDX agreement scores

Similar to the previous work, we developed the HDX agreement score based on the observed correlation between the flexibility and solvent exposure metrics and the experimental HDX-NMR protection factors (Marzolf et al., 2021). However, here, the quantitative protection factors were incorporated directly into the scoring function. From the crystal structures of the ten proteins, for each residue

with experimental PF (total of 431), four different parameters (NC, RelSASA, OS, and HB) were calculated. For each metric, the correlation between the parameters and PF of ten proteins was examined with linear regression lines as shown in [Equation 2](#).

$$\text{Predicted parameter} = \log(\text{PF}) * \alpha + \beta \quad (\text{Equation 2})$$

The trends between each parameter and $\log(\text{PF})$ matched our hypotheses (sign of slope, α), thus they were used to score predicted structures based on HDX agreement. To score sampled structures from Rosetta *ab initio* or RosettaCM, we first used Rosetta to calculate the four parameters (NC, RelSASA, OS, and HB) for each of the residues with HDX PF. Next, the values of the parameters were predicted based on the PF (using [Equation 2](#)). The slopes and y-intercepts of the linear regressions for the four metrics are reported in [Table S3](#). The HDX agreement score was developed to score residues by quantifying the absolute differences (Δ_i) between the Rosetta calculated values and the predicted values of a residue i using the corresponding PF. In short, residues with a poor agreement were scored as 0, residues with strong agreement were scored as -1, and a linear function was used for those between. The specific form of the score function is shown in [Equation 3](#).

$$\text{Score per residue}_i = \begin{cases} -1, \Delta_i \leq c_1 \\ \frac{\Delta_i}{2} - \left(\frac{c_1 + c_2}{4}\right) - 0.5, c_1 < \Delta_i \leq c_2 \\ 0, c_2 < \Delta_i \end{cases} \quad (\text{Equation 3})$$

For each metric, there were two cutoffs used to determine whether the residue followed the HDX agreement. Cutoff 1 (c_1) was the rewarding cutoff. Specifically, the residue was fully rewarded with -1, if Δ_i was less than c_1 , which showed that the observed parameters were consistent with the predicted parameters. Values of c_1 for each different metric were determined based on the range of numerical values of each metric ($c_1 = 1.0$ for NC, $c_1 = 0.1$ for RelSASA, $c_1 = 0.2$ for OS, and $c_1 = 0.2$ for HB). Cutoff 2 (c_2) was the non-rewarding cutoff. If Δ_i was greater than c_2 , the calculated parameters were inconsistent with the predicted values. Hence, the residue would not be rewarded (0). From the standard deviations of native models of 10 proteins for NC, RelSASA, OS, and HB (2.31 for NC, 0.278 for RelSASA, 0.623 for OS, and 0.836 for HB), values of c_2 were determined ($c_2 = 2.0$ for NC, $c_2 = 0.3$ for RelSASA, $c_2 = 0.6$ for OS, and $c_2 = 0.8$ for HB). If Δ_i fell between c_1 and c_2 , the residue would be linearly rewarded based on Δ_i as shown in [Equation 3](#).

Using this scoring algorithm, the score per residue for each parameter would range between -1 for a fully rewarded residue to 0 for a non-rewarded residue. For a model, the HDX component score (S) for each individual parameter was defined as the sum of the residue scores for all residues with experimental PF, as shown in [Equation 4](#).

$$S = \sum_i^{\# \text{ residues with PF}} \text{Score per residue}_i \quad (\text{Equation 4})$$

By including the HDX agreement score, the HDX score was defined as the linear combination of the REF2015 Rosetta score (RS) and model score (S) of each metric, as showed in [Equation 5](#). The HDX terms in [Equation 5](#) are defined as the HDX component of the score.

$$\text{HDX Score} = RS + 2 * S(\text{NC}) + 3 * S(\text{RelSASA}) + 4 * S(\text{OS}) + 3 * S(\text{HB}) \quad (\text{Equation 5})$$

Confidence metric

A confidence metric was developed to assess the extent of confidence in near-native model generation without knowledge of a crystal structure. The confidence metric was defined as the average RMSD of the top 10 scoring models to the top scoring model. If the confidence metric was less than 6 Å, the prediction was considered to be the high confidence. For these proteins, the predicted model had a high probability to be a near-native model. On the other hand, if the confidence metric was greater than 6 Å, the prediction was considered low confidence, such that a near-native model was not expected to be predicted.

QUANTIFICATION AND STATISTICAL ANALYSIS

The correlation between the flexibility and solvent exposure metrics and the experimental HDX-NMR protection factors of 431 residues, for which we had protection factors, were examined using linear regression ([Figure 1](#)). The R^2 values were reported in [Figure 1](#), while the slopes and y-intercepts were reported in [Table S3](#). The standard deviations of native models of 10 proteins for NC, RelSASA, OS, and HB of 431 residues were calculated and reported in the [method details](#) section. All calculations and statistical analysis were performed using Python v3.8.